Cell Reports

Article

Loss of MTCH-1 suppresses age-related proteostasis collapse through the inhibition of programmed cell death factors

Graphical abstract

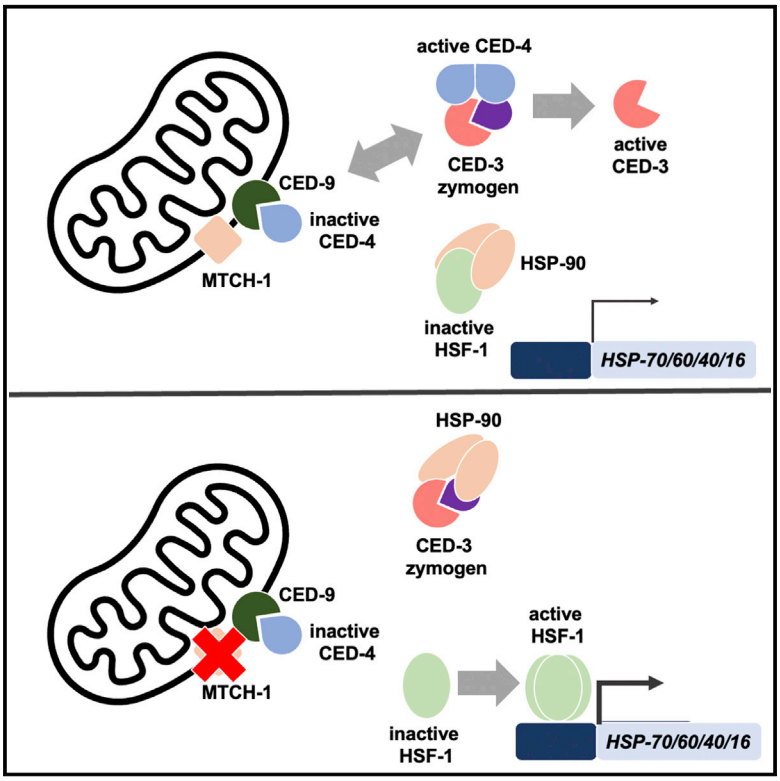

Highlights

- Reduced MTCH-1 function enhances proteostasis capacity
- Loss of MTCH-1 promotes longevity without compromising growth or fecundity
- MTCH-1 depletion enhances HSF-1 activity by inhibiting CED-4/CED-3 caspases
- Inhibiting MTCH-1 shifts HSP-90 activity toward CED-3 and derepresses HSF-1

Authors

Yahyah Aman, Annmary Paul Erinjeri, Nikolaos Tataridas-Pallas, Rhianna Williams, Rachel Wellman, Hannah Chapman, John Labbadia

Correspondence

j.labbadia@ucl.ac.uk

In brief

In this work, Aman et al. demonstrate that reducing levels of the mitochondrial outer membrane protein MTCH-1 can maintain protein homeostasis and promote tissue health in aged tissues. These beneficial effects are achieved through inhibition of programmed cell death factors, which increases activity of the transcription factor HSF-1.

Aman et al., 2022, Cell Reports *41*, 111690
November 22, 2022
https://doi.org/10.1016/j.celrep.2022.111690

CellPress

Cell Reports

CellPress
OPEN ACCESS

Article

Loss of MTCH-1 suppresses age-related proteostasis collapse through the inhibition of programmed cell death factors

Yahyah Aman,[1,2] Annmary Paul Erinjeri,[1,2] Nikolaos Tataridas-Pallas,[1,2] Rhianna Williams,[1] Rachel Wellman,[1] Hannah Chapman,[1] and John Labbadia[1,3,*]

[1]Institute of Healthy Ageing, Department of Genetics, Evolution and Environment, Division of Biosciences, University College London, London, WC1E 6BT, UK

[2]These authors contributed equally

[3]Lead contact

*Correspondence: j.labbadia@ucl.ac.uk

https://doi.org/10.1016/j.celrep.2022.111690

SUMMARY

The age-related loss of protein homeostasis (proteostasis) is at the heart of numerous neurodegenerative diseases. Therefore, finding ways to preserve proteome integrity in aged cells may be a powerful way to promote long-term health. Here, we show that reducing the activity of a highly conserved mitochondrial outer membrane protein, MTCH-1/MTCH2, suppresses age-related proteostasis collapse in *Caenorhabditis elegans* without disrupting development, growth, or reproduction. Loss of MTCH-1 does not influence proteostasis capacity in aged tissues through previously described pathways but instead operates by reducing CED-4 levels. This results in the sequestration of HSP-90 by inactive CED-3, which in turn leads to an increase in HSF-1 activity, transcriptional remodeling of the proteostasis network, and maintenance of proteostasis capacity with age. Together, our findings reveal a role for programmed cell death factors in determining proteome health and suggest that inhibiting MTCH-1 activity in adulthood may safeguard the aging proteome and suppress age-related diseases.

INTRODUCTION

The ability to maintain a healthy proteome is crucial for the long-term function of all tissues.[1] However, a decline in the capacity to maintain protein homeostasis (proteostasis) with age is observed in worms, flies, mice, and humans.[2] This gives rise to the appearance and persistence of misfolded and aggregated proteins (proteostasis collapse), which in turn gives rise to many disorders, including dementia, muscle wasting, liver disease, and diabetes.[3] Therefore, identifying pathways and mechanisms that can subdue the accumulation of protein aggregates in aged tissues may be a powerful way to suppress the onset and progression of many age-associated diseases.

Given the ramifications associated with the accumulation of aberrant protein species, cells possess many sophisticated mechanisms for maintaining proteostasis.[2] The components of these protein quality control mechanisms are integrated into the proteostasis network (PN), a collection of folding, trafficking, and degradation pathways that span the cell and act to surveil the proteome in order to neutralize any misfolded, mislocalized, or aggregated proteins that arise.[2] Although the PN robustly safeguards the proteome early in life, the capacity of the PN to maintain proteostasis declines abruptly during adulthood in worms, flies, and mice, leaving cells and tissues more vulnerable to the accumulation of toxic protein species with age.[4–7]

Attempts to understand the basis of proteostasis collapse in the nematode worm *Caenorhabditis elegans* have revealed that proteostasis capacity declines as animals commit to reproductive maturity.[8,9] This is preceded by a rapid decline in the ability of the transcription factor HSF-1 to drive the expression of PN genes, most notably those encoding for small heat shock proteins (sHSPs) and HSP-70 family members.[8] Over-expression and knockdown of HSF-1 suppress and enhance age-related proteostasis collapse, respectively, suggesting that finding ways to maintain HSF-1 activity throughout life could preserve proteostasis capacity and prolong healthy tissue function with age.[10–13]

Several studies have shown that the long-term activity of HSF-1 is determined by pathways operating during development and that the removal of germline stem cells (GSCs), inhibition of electron transport chain activity, reduction of food intake, and destabilization of eggshell integrity, can all maintain proteostasis in an HSF-1-dependent manner.[8,9,14–17] These findings demonstrate that multiple pathways act early in life to couple long-term HSF-1 activity with reproductive potential and nutritional status during development. This raises two important questions: (1) What is the full complement of pathways acting early in life to control the long-term activity of HSF-1? and (2) Can HSF-1 activity and proteostasis capacity be maintained without detrimental effects on early-life physiology?

Here, we demonstrate that the highly conserved outer mitochondrial membrane protein, MTCH-1/MTCH2, is a negative regulator of HSF-1 activity in adulthood. Reducing MTCH-1 levels increases HSF-1 activity and enhances proteostasis capacity through a mechanism that is distinct from previously reported proteostasis modifying pathways. Surprisingly, these effects are not associated with growth defects, developmental delay, or altered fecundity and occur through inhibition of programmed cell death (PCD) factors and reduced HSP-90 activity. Our findings suggest that maintenance of proteostasis capacity with age can be uncoupled from immediate effects on fitness by targeting PCD factors and HSP-90 in adulthood.

RESULTS

Reducing MTCH-1 levels prevents the programmed loss of stress resistance during early adulthood

Using an unbiased genome-wide RNAi screening approach, we previously identified *mtch-1* (which encodes a highly conserved transporter in the mitochondrial outer membrane) as a suppressor of thermal stress resistance in reproductively mature *C. elegans* adults.[14] To determine whether knockdown of *mtch-1* generally increases stress resistance at any life stage, or specifically suppresses the loss of stress resistance in early adulthood, we grew animals on empty vector (EV) control (L4440) or *mtch-1(RNAi)* and measured resistance to heat, endoplasmic reticulum (ER) (tunicamycin), and oxidative (paraquat) stress on days 1 and 3 of adulthood (the window during which stress resistance declines during *C. elegans* adulthood).[8,18]

Knockdown of *mtch-1* enhanced resistance to both heat and tunicamycin treatment on day 3 but not day 1 of adulthood (resistance to heat stress was maintained until day 7 of adulthood) and increased lifespan without causing developmental delay, reduced body size, or altered reproductive output/duration (Figures 1A, 1B, 1D, S1A–S1D, S1F, and S1G). However, *mtch-1(RNAi)* did not affect sensitivity to paraquat treatment, which increased between days 1 and 3 of adulthood in control animals (Figure 1C). The increase in paraquat resistance observed in day 3 adult animals is contrary to previous observations[8] and possibly reflects a shift in paraquat dose and exposure method (solid versus liquid media).

Increased stress resistance and lifespan were also observed in *mtch-1(ok1800)* knockout (KO) mutants (Figures 1E and 1F). However, in contrast to *mtch-1(RNAi)*-treated worms, *mtch-1(ok1800)* animals were small, lean, and sterile compared with wild-type controls (Figure S1B), phenotypes that were copied in the progeny of parents exposed to *mtch-1(RNAi)* from the mid-L4 stage (Figure S1E). In addition, *mtch-1(ok1800)* KO mutants exhibited a modest reduction in pharyngeal pumping rate (feeding), which was not observed upon *mtch-1(RNAi)* (in which pumping was moderately increased) (Figures S1H and S1I). Therefore, we decided to focus our subsequent experiments on *mtch-1(RNAi)*-treated animals.

Removal of GSCs and reduced feeding have both been shown to prevent the programmed loss of stress resistance during early *C. elegans* adulthood.[8,15] To test whether *mtch-1(RNAi)* may be enhancing stress resistance by engaging the same pathways, we tested resistance to heat stress in germline stem cell-deficient (*glp-1*) and dietary-restricted (DR) (*eat-2*) mutants. Knockdown of *mtch-1* enhanced stress resistance in *glp-1* and *eat-2* mutants to the same extent as in wild-type worms (Figures S1J and S1K), suggesting that reduced MTCH-1 activity prevents the programmed loss of stress resistance in early adulthood independently of previously described GSC- and DR-proteostasis pathways.[8,9,15,16]

Loss of MTCH-1 enhances proteostasis capacity and selectively suppresses proteotoxicity across tissues

To ascertain whether the maintenance of stress resistance upon knockdown of MTCH-1 is due to enhanced proteostasis capacity, we measured the aggregation propensity of previously described polyglutamine:YFP (PolyQ:YFP)-based proteostasis sensors in the body wall muscle or intestine of control or *mtch-1(RNAi)*-treated animals.[19,20] Knockdown of *mtch-1* suppressed age-related polyglutamine aggregation in both tissues (Figures 2A, 2B, and S2A); however, this did not correspond to a reduction in age-related polyQ toxicity in muscles (Figure 2C). To explore the ability of *mtch-1(RNAi)* to suppress age-related proteotoxicity caused by other substrates and in other tissues, we used previously described models to measure metastable myosin (*unc-54ts*), amyloid beta 1–42 ($A\beta_{1-42}$) and polyQ-induced toxicity in aging muscles and neurons.[4,21,22] In contrast to effects on polyQ, reduced MTCH-1 activity suppressed the toxicity caused by misfolded myosin and $A\beta_{1-42}$ in body wall muscle cells (Figures 2D and S2B). Furthermore, despite not influencing polyQ toxicity in muscles, *mtch-1(RNAi)* did suppress polyQ and $A\beta_{1-42}$ toxicity in neurons (Figures 2E and 2F). Together, these data suggest that reducing MTCH-1 levels maintains proteostasis capacity in early adulthood and selectively suppresses age-related proteotoxicity across tissues.

Knockdown of MTCH-1 enhances stress resistance through an HSF-1-mediated cytosolic unfolded protein response

Given that *mtch-1(RNAi)* can protect against age-related proteotoxicity, we next wanted to investigate how reduced MTCH-1 activity alters the composition of the PN during adulthood. In wild-type animals, the loss of proteostasis capacity in early adulthood is preceded by the programmed repression of inducible proteostasis pathways in the cytosol (heat shock response [HSR]), ER(UPR^{ER}), and mitochondria (UPR^{mt}) as animals commit to reproduction.[8,18] To ascertain whether *mtch-1(RNAi)* maintains proteostasis capacity by preserving inducible PN pathways, we measured the expression of canonical HSR (*hsp-16.11*, *hsp-70*, *hsp-70b/F44E5.4*, and *hsp-1*), UPR^{ER} (*hsp-4*), and UPR^{mt} (*hsp-6*) genes on days 1 and 3 of adulthood following exposure to basal (20°C) or heat shock conditions (33°C, 30 min). As expected, the ability to induce HSR and UPR genes declined sharply between days 1 and 3 of adulthood in control animals (Figures S3A–S3F). However, this phenomenon was not suppressed by treatment with *mtch-1(RNAi)* (Figures S3A–S3F), suggesting that reducing MTCH-1 activity preserves proteostasis capacity in aged tissues without preventing the repression of stress response pathways in early adulthood.

We next asked whether the maintenance of proteostasis capacity emerges from changes in the basal expression of

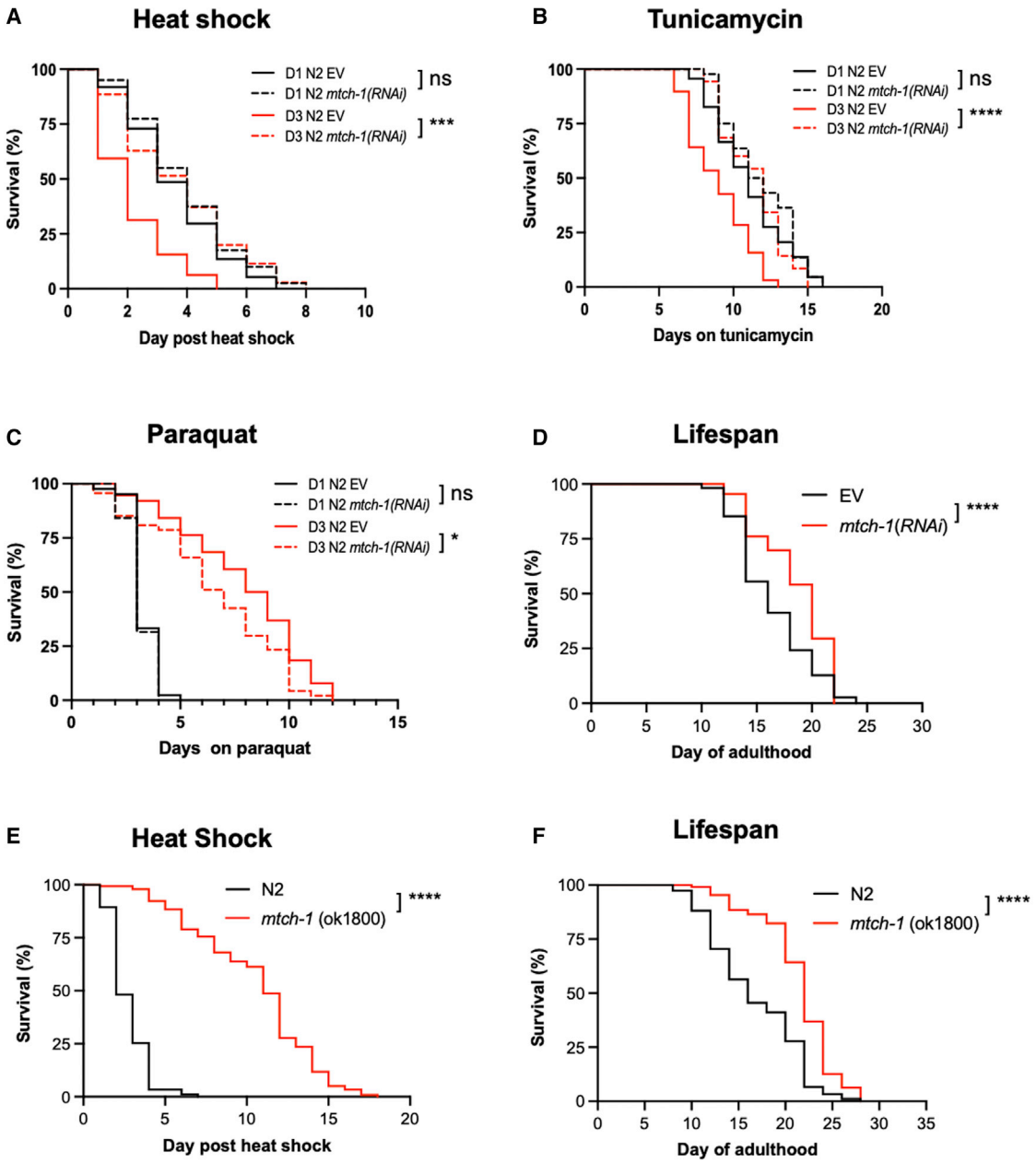

Figure 1. Reducing MTCH-1 levels prevents the programmed loss of stress resistance during early adulthood

(A–C and E) Survival following exposure to (A and E) transient heat shock (35°C for 4 h), (B) tunicamycin (50 μg/mL), or (C) paraquat (10 mM) on day 1 or 3 of adulthood. Wild-type (N2) animals were grown on EV (L4440) or *mtch-1(RNAi)*.

(D and F) Lifespan of (D) wild-type animals grown on EV (L4440) or *mtch-1(RNAi)* or (F) wild-type and *mtch-1(ok1800)* knockout mutants, at 20°C.

Statistical significance in (A)–(F) was calculated using the Mantel-Cox log rank test. ns, not significant ($p > 0.05$); *$p < 0.05$, ***$p < 0.001$, and ****$p < 0.0001$. Three independent trials were performed for each survival experiment. Full statistics for all stress resistance and lifespan trials (including n values) can be found in Table S1. See also Figure S1.

inducible PN genes. We used RNA sequencing (RNA-seq) to compare the expression of core cytosolic, ER, and mitochondrial PN genes in control and *mtch-1(RNAi)*-treated animals on day 3 of adulthood.

Knockdown of *mtch-1* resulted in the induction of a subset of cytosolic PN genes (*hsp-16.2*, *hsp-16.41*, *hsp-70*, *hsp-70b(F44E5.4/5)*, *unc-23*, *dnj-19*, *cct-1*, *hsp-110*, *aip-1*) that was confirmed by qRT-PCR and observed on day 3, but not day 1, of adulthood (Figures 3A–3G, S3G–S3J, and S4B). In addition, we found that the levels of HSF-1 associated with the promoters of up-regulated genes was increased in response to *mtch-1(RNAi)* treatment (Figure 3H) and that *hsf-1*, but not *daf-16*, is

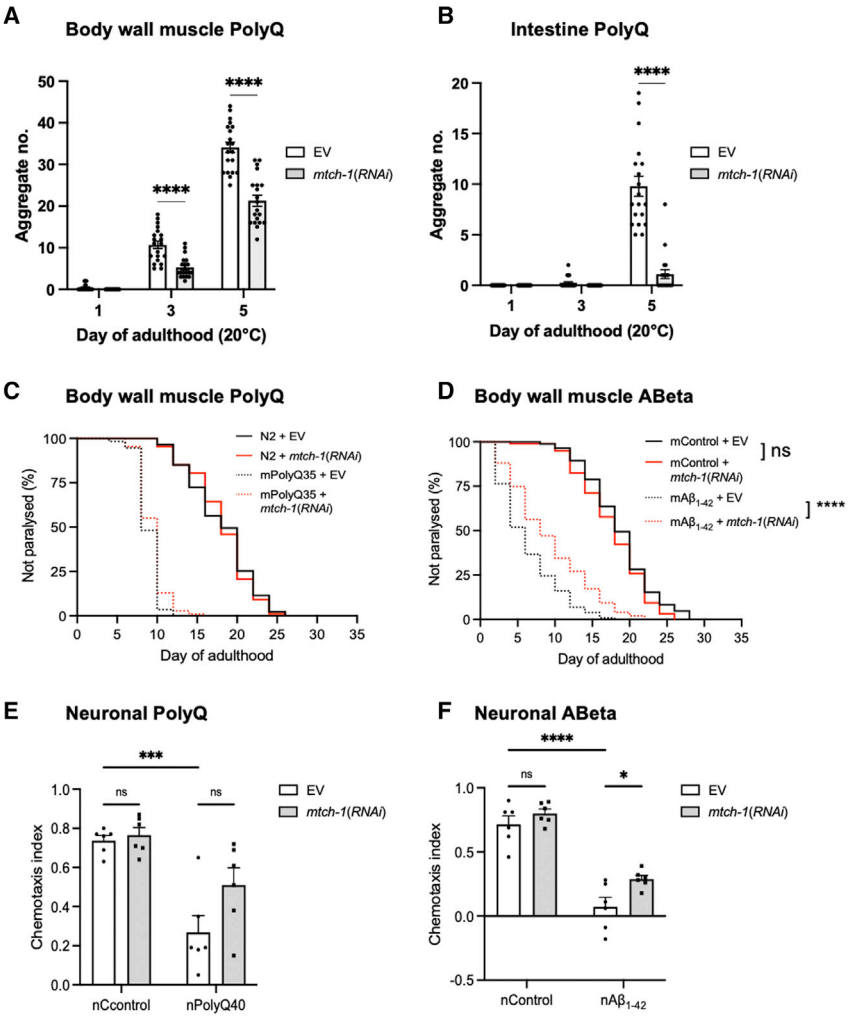

Figure 2. Reduced MTCH-1 activity suppresses protein aggregation and age-related proteotoxicity across tissues

(A and B) Number of polyglutamine::YFP aggregates present in the (A) body wall muscle (Q35::YFP) or (B) intestine (Q44::YFP) on different days of adulthood in worms grown on EV (L4440) control or *mtch-1(RNAi)* plates. Values plotted are the mean ($n \geq 19$ animals per group).

(C and D) Proportion of control, (C) PolyQ35, or (D) $A\beta_{1-42}$ animals exhibiting paralysis at different days of adulthood following growth on EV (L4440) control or *mtch-1(RNAi)* plates ($n > 100$ animals per group).

(E and F) Chemotaxis index on day 3 of adulthood of control worms and animals expressing (E) PolyQ(40)::YFP or (F) $A\beta_{1-42}$ in neurons following growth on EV (L4440) control or *mtch-1(RNAi)* plates. Values plotted are the mean of 6 biological replicates.

Statistical significance was calculated using two-way ANOVA with post-analysis pairwise comparison of groups (A, B, E, and F) or the Mantel-Cox log rank test (C and D). Error bars denote SEM. ns, not significant ($p > 0.05$); *$p < 0.05$ and ****$p < 0.0001$. See also Figure S2.

required for increased stress resistance upon *mtch-1(RNAi)* and knockout (Figures 3I, 3J, S3K, and S3L). Together, these data demonstrate that reduced MTCH-1 activity protects against age-related proteostasis collapse through increased HSF-1 activity and the up-regulation of a distinct subset of cytosolic PN genes.

Knockdown of MTCH-1 does not alter lipid homeostasis

If knockdown of *mtch-1* does not alter fecundity or feeding, how then, does it enhance stress resistance and maintain proteostasis in aged tissues? In mammals and worms, MTCH-1/MTCH2, has been proposed to control lipid homeostasis and to positively regulate apoptosis.[23,24] In addition, MTCH-1 resides within the mitochondrial outer membrane and compromised mitochondrial function is linked to maintenance of proteostasis and increased lifespan.[14] Therefore, we reasoned that the maintenance of proteostasis capacity downstream of *mtch-1(RNAi)* could stem from the disruption of one, or all, of these processes.

RNA-seq analysis revealed 153 down-regulated and 437 up-regulated genes (1.5-fold or greater) on day 3 of adulthood in response to *mtch-1(RNAi)* (Figure S4A). Functional and pathway enrichment analysis revealed that up-regulated genes were enriched for roles in nervous system development and sphingolipid metabolism, while down-regulated genes were enriched for roles in pathogen defense and fatty acid metabolism (Figures S4C and S4D). To test whether depleted fat stores could underlie enhanced proteostasis capacity, we measured lipid levels in control and MTCH-1 compromised animals using oil red O (ORO) staining. Consistent with previous studies,[24] we find that levels of ORO staining were greatly reduced in *mtch-1(ok1800)* knockout animals (Figure S4E). However, ORO staining was unaltered upon exposure to *mtch-1(RNAi)* (Figure S4E), suggesting that a gross alteration in fat metabolism or lipid stores does not underlie enhanced proteostasis capacity in response to *mtch-1* knockdown.

Knockdown of MTCH-1 does not enhance proteostasis capacity through impaired ETC activity or altered mitochondrial dynamics

Given that the human orthologue of MTCH-1, MTCH2, is a mitochondrial outer membrane protein with a role in mitochondrial fusion, we next examined the impact of *mtch-1(RNAi)* on mitochondrial function and dynamics. Unlike ETC impairment (*cox-6c[RNAi]*), *mtch-1(RNAi)* did not induce a mitochondrial unfolded protein response, reduce ATP levels, or impair respiration but did increase membrane potential and promote mitochondrial fusion compared with control animals (Figures 4A–4E). In addition, *mtch-1(RNAi)* enhanced stress resistance on day 3 of adulthood in ETC (*isp-1;ctb-1*), fusion (*fzo-1*) and fission (*drp-1*) compromised worms to the same

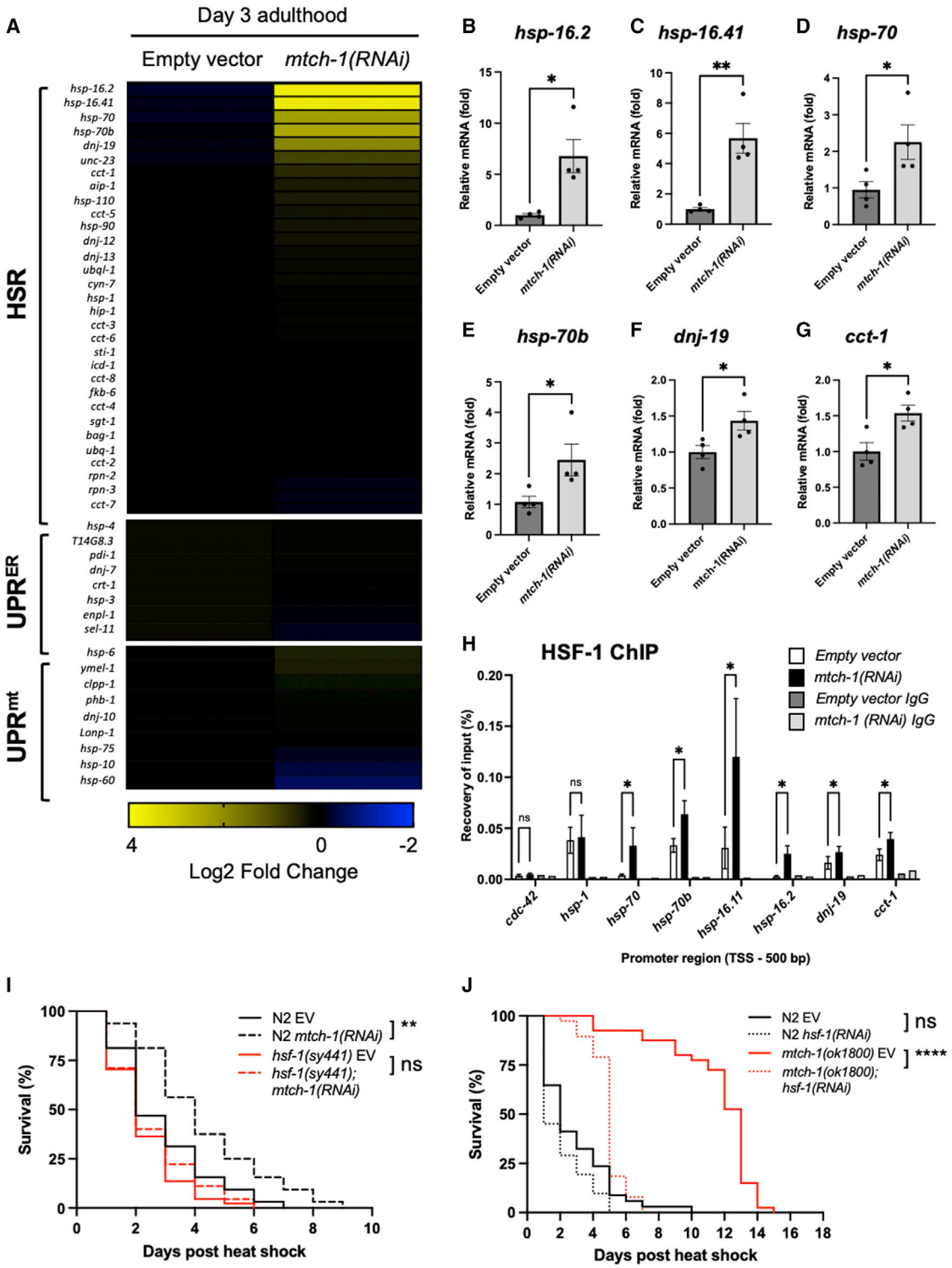

Figure 3. Knockdown of MTCH-1 enhances stress resistance through an HSF-1-mediated cytosolic unfolded protein response

(A) RNA-seq analysis of the basal expression of HSR, UPR^{ER}, and UPR^{mt} genes on day 3 of adulthood in wild-type (N2) animals grown on EV (L4440) control or *mtch-1(RNAi)*. Mean $\log_2$ fold change between groups is plotted for each gene (n = 4 biological replicates per group).

(B–G) Relative expression of (B) *hsp-16.2*, (C) *hsp-16.41*, (D) *hsp-70*, (E) *hsp-70b(F44E5.4/5)*, (F) *dnj-19*, and (G) *cct-1* mRNA on day 3 of adulthood in wild-type animals grown on EV (L4440) control or *mtch-1(RNAi)*. Data are the mean of 4 biological replicates.

(legend continued on next page)

extent as was observed in wild-type controls (Figures 4F and 4G). Finally, we observed that the increased stress resistance of *mtch-1(RNAi)* worms was not dependent on *let-92*, which we have previously shown is necessary for increased proteostasis capacity upon ETC impairment[17] (Figure S4F). Together, our results indicate that MTCH-1 has important roles in mitochondrial function, mitochondrial fusion and lipid metabolism in *C. elegans*. However, changes in these processes do not appear to underlie the enhanced proteostasis capacity of *mtch-1(RNAi)* worms.

Reduced MTCH-1 activity maintains proteostasis through inhibition of the programmed cell death pathway

Given that MTCH2 positively regulates apoptosis in mammals, we hypothesized that reduced MTCH-1 activity may maintain proteostasis through the inhibition of programmed cell death factors. In *C. elegans*, apoptosis is regulated through the *egl-1-ced-9-ced-4-ced-3* axis and loss (*egl-1*, *ced-4*, or *ced-3*) or gain (*ced-9*) of function mutations in these genes block apoptosis.[25] We found that *ced-9(1050 gof)*, *ced-4(n1162 lof)*, and *ced-3(n717 lof)* mutants all enhanced stress resistance in day 3 adult animals, whereas *egl-1(ko)* mutants did not (Figures 5A–5D). Importantly, *mtch-1(RNAi)* did not further increase stress resistance in *ced-9*, *ced-4*, or *ced-3* mutants but did increase stress resistance in *egl-1(n3330 lof)* mutants (Figures 5A–5D). These effects were not due to reduced *mtch-1* expression in *ced* mutants (Figure S4A) and suggest that the loss of MTCH-1 enhances stress resistance through the inhibition of programmed cell death.

To determine whether the prevention of cell death was necessary for MTCH-1 depletion to enhance stress resistance, we counted the number of NSM neurons present in adult animals using a HIS-24::GFP reporter line[26] and scored the number of germline apoptotic corpses present in adulthood using a CED-1::GFP reporter strain.[27] NSM number and frequency of CED-1::GFP halos increase upon inhibition of developmental apoptosis (DA; embryo and early larvae) and physiological apoptosis (adult germline), respsectively.[25] Our experiments revealed that *mtch-1(RNAi)* had no effect on NSM number or frequency of CED-1::GFP cells in adulthood (Figures S4B and S4C). Together, these data suggest that the maintenance of proteostasis capacity downstream of *mtch-1(RNAi)* comes about from the inhibition of canonical PCD pathway factors but does not require the prevention of cell death per se.

To determine whether the increased stress resistance observed upon inhibition of the core PCD pathway is associated with increased HSF-1 activity and enhanced proteostasis capacity, we knocked down *ced-3* and *ced-4* by RNAi and assessed the impact on polyglutamine aggregation in the body wall muscle and intestine with age. We found that RNAi against *ced-4*, but not *ced-3*, suppressed age-related polyglutamine aggregation in both tissues (Figures 5E and 5F). In addition, *ced-3(n717)* mutants exhibited increased expression of HSF-1 target genes on day 3 of adulthood (Figures S5D–S5G), and the increased stress resistance of *ced-3(n717)* and *ced-4(n1162)* mutants was *hsf-1* dependent (Figures 5G and 5H). The failure of *ced-3(RNAi)* to suppress polyQ aggregation suggests that it is the maintenance of an inactive form of CED-3 (as is the case in the n717 mutant) rather than loss of CED-3 (as is the case with RNAi), which enhances proteostasis capacity.[28] In contrast, both *ced-4(n1162)* and *ced-4(RNAi)* lead to a depletion of CED-4 protein.[29] Together, our data suggest that reduced *mtch-1* levels inhibit the activity of core PCD factors in adulthood, and that this in turn results in increased HSF-1 activity and protection from age-related protein aggregation.

MTCH-1 knockdown enhances HSF-1 activity by reducing CED-4 levels and inhibiting HSP-90 activity

How then does loss of MTCH-1 inhibit the PCD pathway, and how does this in turn regulate HSF-1 activity? Given that MTCH-1, CED-9, and CED-4 are all associated with the mitochondrial outer membrane, we reasoned that the loss of MTCH-1 may alter the stability and/or activity of CED-9 and/or CED-4. To test this, we measured CED-3, CED-4, and CED-9 levels following knockdown of *mtch-1* using worms expressing CED-3::GFP from the *ced-3* promoter,[30] worms expressing CED-4::GFP from the *ced-4* promoter,[31] or antibodies against CED-9 and MTCH-1. We found that *mtch-1(RNAi)* reduced MTCH-1 levels by approximately 75% but did not alter levels of CED-3::GFP or CED-9 (Figures 6A and 6B). However, *mtch-1(RNAi)* was associated with reduced levels of CED-4::GFP (Figures 6A and 6B). In contrast, MTCH-1 levels were not altered in *ced-4(n1162)* mutants (Figure 6C). These data suggest that the loss of MTCH-1 interacts with the PCD machinery by reducing CED-4 stability.

Next, we asked how loss of MTCH-1 may be augmenting HSF-1 activity. We first asked whether *mtch-1(RNAi)* increased levels of HSF-1 or decreased levels of HSP-90 and HSP-70, two canonical negative regulators of HSF-1 activity.[32] Levels of *hsf-1* mRNA as well as HSF-1, HSP-70, and HSP-90 protein, were unaltered in *mtch-1(RNAi)*-treated worms (Figures 6D and S6A–S6E). Given that HSP-90 has been reported to associate with apoptosis regulators in mammalian cells,[33] we hypothesized that an increase in HSP-90 binding to CED-3 or CED-4 in response to *mtch-1(RNAi)* could titrate HSP-90 away from intracellular complexes that repress HSF-1 activity.

We were able to immunoprecipitate CED-3::GFP and CED-4::GFP at comparable levels from both control and

(H) Relative levels of HSF-1::GFP bound to promoters of proteostasis genes or *cdc-42* on day 3 of adulthood following exposure to EV (L4440) controls or *mtch-1(RNAi)*. Data are the mean of 4 biological replicates.

(I and J) Survival following heat shock (35°C, 4 h) on day 3 of adulthood of (I) wild-type (N2) and *hsf-1(sy441)* mutant animals exposed to EV (L4440) control or *mtch-1(RNAi)* or (J) wild-type and *mtch-1(ok1800)* worms exposed to EV (L4440) control or *hsf-1(RNAi)*. Three independent trials were performed per stress resistance experiment. Trials were run in parallel with *daf-16(mu86)* and *daf-16(RNAi)* animals (Figures S3K and S3L).

Error bars denote SEM in all cases. Statistical significance was calculated using unpaired, two-tailed Student's t test (B–H) or the Mantel-Cox Log rank test (I and J). Full statistics for all stress resistance and lifespan trials (including n values) can be found in Table S1 ns, not significant ($p > 0.05$); *$p < 0.05$, **$p < 0.01$, and ****$p < 0.0001$. See also Figure S3.

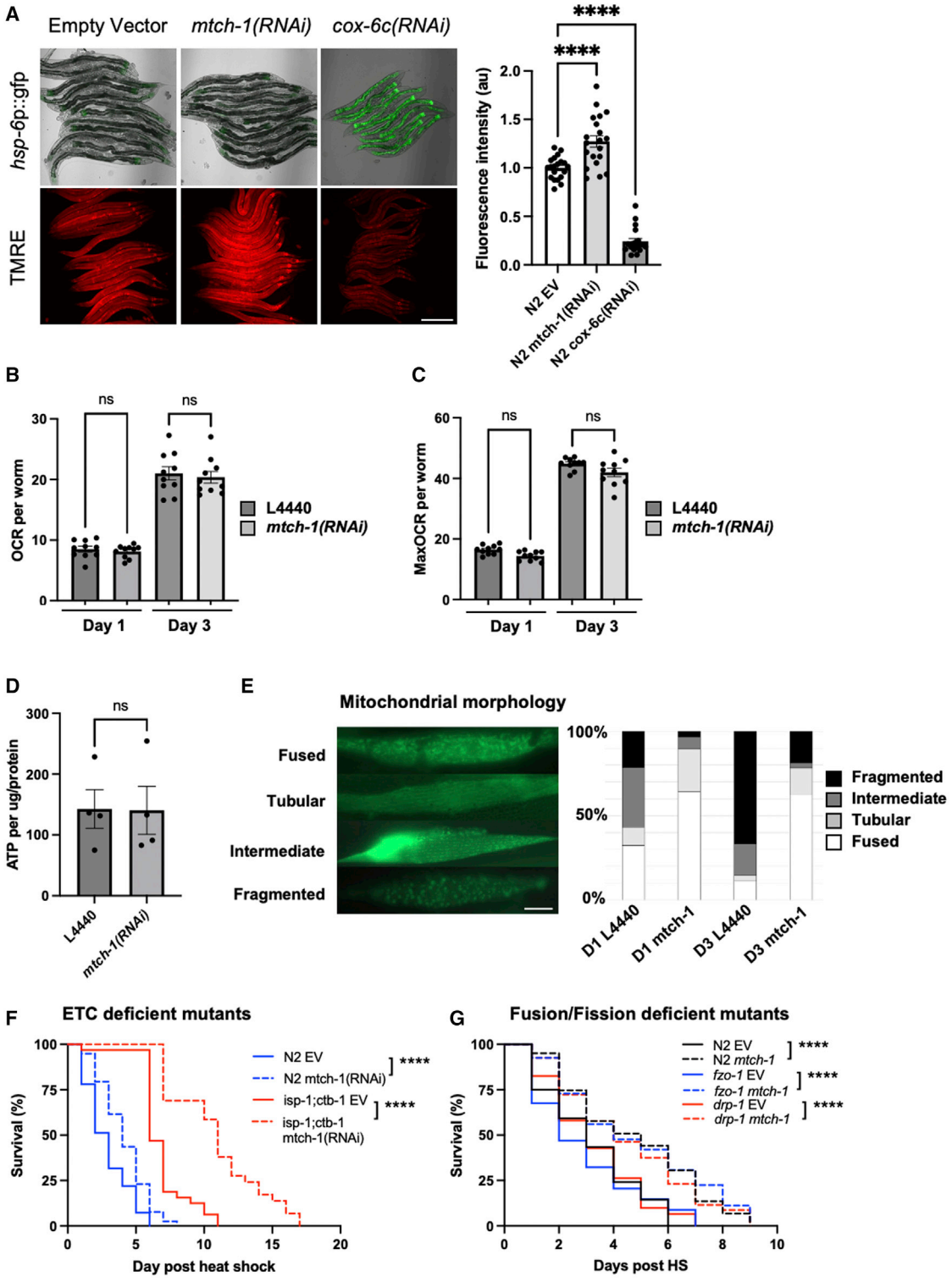

Figure 4. Knockdown of MTCH-1 does not enhance proteostasis capacity through impaired ETC activity or altered mitochondrial dynamics

(A) Representative images of *hsp-6p::gfp* worms or wild-type TMRE-treated worms following growth on EV (L4440) control, *mtch-1(RNAi)*, or *cox-6c(RNAi)*. Mean fluorescence intensity of TMRE staining (n ≥ 18 animals per group) was measured and plotted. Scale bar, 250 μM.

(B and C) Basal (B) and maximal (C) oxygen consumption rate (OCR) of day 1 and day 3 adult worms following growth on EV (L4440) control or *mtch-1(RNAi)*. Mean values (n = 10 replicates per group) are plotted.

(legend continued on next page)

mtch-1(RNAi)-treated worms using an anti-GFP antibody, but not IgG alone (Figures 6E and 6F). In addition, we were able to recover HSP-90 but not HSP-70 with both CED-4::GFP and CED-3::GFP, but not from worms expressing GFP alone (Figure S6F). Crucially, we found that the levels of HSP-90 recovered with CED-3::GFP, but not CED-4::GFP, increased in response to *mtch-1(RNAi)* (Figures 6E and 6F), suggesting that HSP-90 is redirected away from existing HSF-1-repressing complexes and toward CED-3 upon loss of MTCH-1.

Finally, we reasoned that if this shift in HSP-90 binding promotes proteostasis capacity through de-repression of HSF-1, then knocking down *hsp-90* in adulthood should copy the effects of *mtch-1(RNAi)* and enhance stress resistance. Furthermore, these effects should not be additive with *mtch-1(RNAi)*. We tested these predictions and found that knocking down *hsp-90* in adulthood did indeed increase stress resistance in wild-type animals but not in *mtch-1(RNAi)*, *ced-3(n717)*, or *ced-4(n1162)* mutants (Figures 6G, 6H, and S6G). Taken together, our data support a model in which MTCH-1 depletion protects the aging proteome by shifting HSP-90 binding away from inhibitory complexes and toward CED-3, thereby derepressing HSF-1 activity and increasing proteostasis capacity.

DISCUSSION

Our work has revealed that MTCH-1 regulates the activity of HSF-1 and proteostasis capacity in adulthood, and that this is dependent on inhibition of the programmed cell death factors, CED-3 and CED-4. Loss-of-function mutations in *ced-3* and *ced-4* have previously been shown to suppress developmental defects caused by tunicamycin treatment.[34] In addition, inhibition of the central apoptosis pathway also reduces death caused by extreme or chronic elevated temperatures on the first day of adulthood, possibly through increased PMK-1 activity.[34–36] Coupled with our findings, these observations suggest that programmed cell death factors have complex secondary roles in determining chronic stress resistance during development, and in facilitating the loss of proteostasis capacity during the transition to reproductive maturity. We consistently observed that loss of CED-4 activity produced the most pronounced increases in stress resistance, suggesting that CED-4 may have important functions during adulthood that extend beyond the regulation of CED-3.

Intriguingly, *ced-3* and *ced-4*, but not *egl-1*, have been shown to be necessary for increased lifespan caused by mitochondrial ROS in *C. elegans*, but are not required for lifespan extension in reduced insulin/insulin-like signaling (*daf-2*), dietary-restricted (*eat-2*) or GSC deficient (*glp-1*) mutants.[35] These findings are reminiscent of our observations that *mtch-1(RNAi)* operates independently of these pathways to maintain proteostasis capacity.

Given that previously identified proteostasis modifying pathways suppress age-related protein aggregation at the expense of slower development, stunted growth, or reduced fecundity, we were surprised to see that loss of MTCH-1 suppresses age-related proteotoxicity without any overt signs of these physiological issues. Other groups have reported that *mtch-1(RNAi)* causes growth and fecundity defects and mitochondrial stress when administered early in life.[24,37,38] Although we observe these effects in *mtch-1(ok1800)* knockout mutants, we do not see them upon *mtch-1(RNAi)*, despite achieving a >90% reduction in *mtch-1* mRNA levels by day 3 of adulthood. These differences most likely arise from differences in the timing of *mtch-1* knockdown, as we found that longer exposure of parents to *mtch-1(RNAi)* resulted in progeny that phenocopied *mtch-1(ok1800)* KO animals. The timing of MTCH-1 depletion may also explain why MTCH-1 perturbation is beneficial in our experiments but reduced *MTCH2* expression is strongly associated with increased risk for Alzheimer's disease (AD) in humans.[39]

In addition to our original RNAi screen for modifiers of stress resistance,[14] MTCH-1 was also identified in RNAi screens for modifiers of polyglutamine aggregation in body wall muscle cells and lifespan.[38,40] Our data are in agreement with these other studies; however, our work also demonstrates that knockdown of *mtch-1* does not suppress polyglutamine-based proteotoxicity in muscles, something that was also observed in a previous study that identified *mtch-1* as an enhancer of polyglutamine aggregation in muscle cells.[40] This is not likely to be due to a general negative effect of *mtch-1(RNAi)* on muscle function, as wild-type motility was unaltered by *mtch-1(RNAi)*, and knockdown of *mtch-1* suppressed proteotoxicity caused by the presence of misfolded myosin or $A\beta_{1-42}$ in muscles. Furthermore, this is unlikely to be due to the way that reduced MTCH-1 activity broadly influences polyglutamine toxicity, as we found that *mtch-1(RNAi)* suppressed both $A\beta_{1-42}$ and polyglutamine toxicity in neurons. One possibility is that MTCH-1 perturbation has detrimental effects on mitochondrial function and energy production that offset the benefits on proteostasis in the muscles of polyglutamine worms, but not in other worm strains. Therefore, although our work identifies MTCH-1/MTCH2 as a potential target to ameliorate age-related protein conformational disease, it is clear that more work is required to understand the selective nature of these effects.

In *C. elegans* and *Drosophila*, the loss of proteostasis capacity early in life is preceded by the repression of heat shock response (HSR) and unfolded protein response (UPR) genes.[8,18,41] Unlike

(D) Relative ATP levels normalized to total protein at day 3 of adulthood in wild-type animals following growth on EV (L4440) control or *mtch-1(RNAi)*. Values plotted are the mean of 4 biological replicates.

(E) Localization of mitochondria targeted GFP in body wall muscles on day 3 of adulthood following growth on EV (L4440) control or *mtch-1(RNAi)*. Mean values (n $\geq$ 10 animals per group) are plotted. Scale bar, 10 μm.

(F and G) Survival of wild-type, (F) *isp-1;ctb-1(qm150;qm189)*, or (G) *fzo-1(cjn20)* and *drp-1*(tm1108) mutants following transient heat shock (35°C, 4 h) on day 3 of adulthood. Worms were maintained at 20°C on EV (L4440) control or *mtch-1(RNAi)* plates. Three independent trials were performed per stress resistance experiment.

All error bars denote SEM. Statistical significance was calculated using one-way ANOVA with post-analysis pairwise comparison of groups (A), two-way ANOVA with post-analysis pairwise comparison of groups (B and C), unpaired two-tailed Student's t test (D), or the Mantel-Cox log rank test (F and G). ns, not significant ($p > 0.05$); ****$p < 0.0001$. Survival statistics for all stress resistance trials related to (F) and (G) (including n values) can be found in Table S1. See also Figure S4.

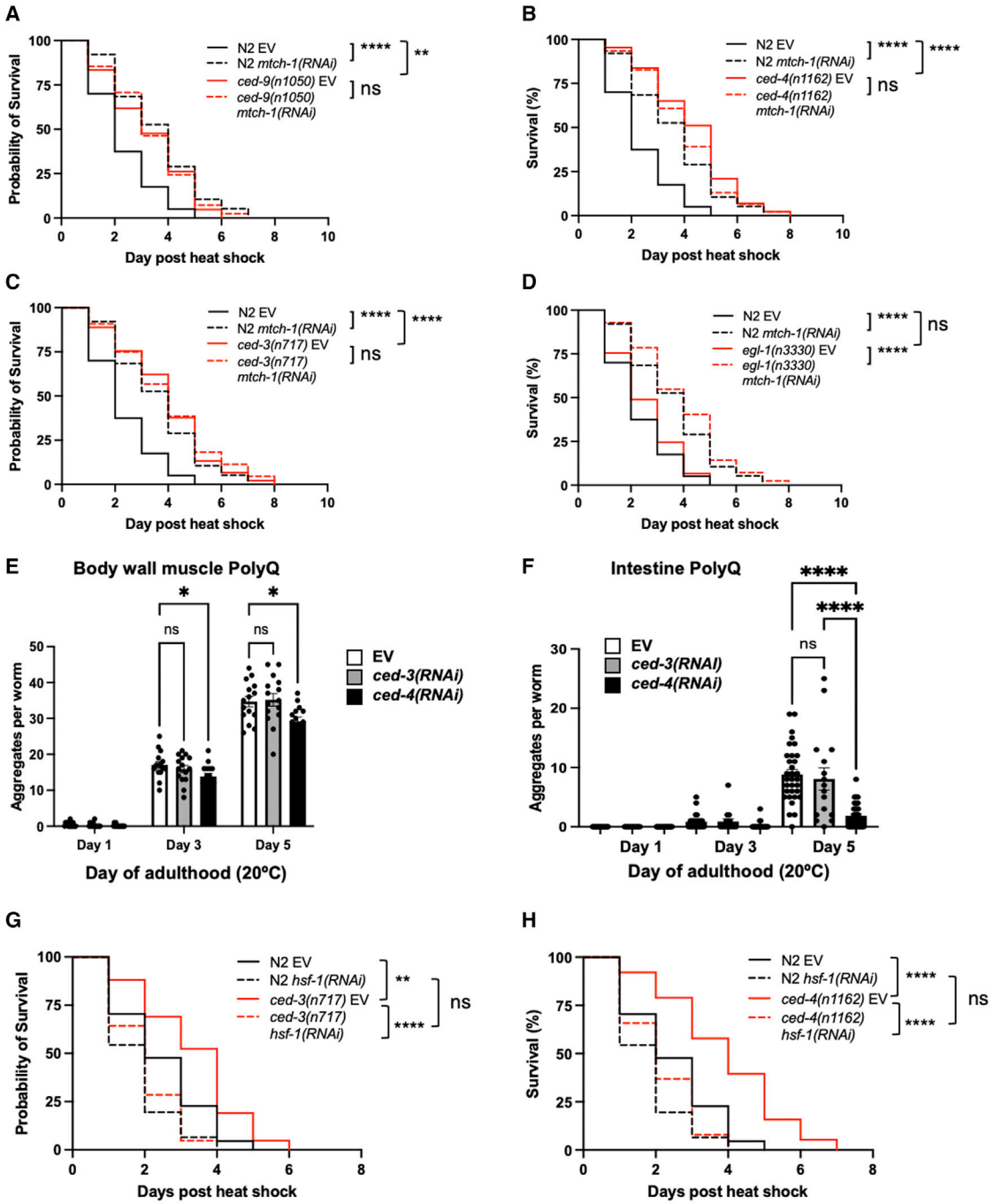

Figure 5. Loss of MTCH-1 does not prevent repression of the heat shock response in early adulthood

(A–D) Survival of wild-type (N2), (A) *ced-9(n1950)*, (B) *ced-4(n1162)*, (C) *ced-3(n717)*, and (D) *egl-1(n3330)* mutants following heat shock (35°C, 4 h) on day 3 of adulthood. Worms were grown on EV (L4440) control or *mtch-1(RNAi)*. All groups were assessed in parallel. Therefore, N2 control groups are the same on all panels. Four independent trials were performed per stress resistance experiment.

(E and F) Polyglutamine (PolyQ) aggregate number on different days of adulthood in (E) body wall muscle cells or (F) intestinal cells of EV (L4440) control or *mtch-1(RNAi)* worms. Values plotted are the mean ($n \geq 15$ animals) of each group.

(G and H) Survival of wild-type (N2) and (G) *ced-3(n717)* or (H) *ced-4(n1162)* animals on day 3 of adulthood following exposure to heat shock (35°C, 4 h). Worms were grown on EV (L4440) control or *hsf-1(RNAi)*. Four independent trials were performed per experiment and trials were conducted in parallel. Therefore, N2 control groups are the same in both panels.

Statistics for all stress resistance trials (including n values) can be found in Table S1. All error bars denote SEM. Statistical significance was calculated using the Mantel-Cox log rank test (A–D, G, and H) or two-way ANOVA with post-analysis pairwise comparison of means (E and F). ns, not significant ($p > 0.05$); *$p < 0.05$, **$p < 0.01$, and ****$p < 0.0001$. See also Figure S5.

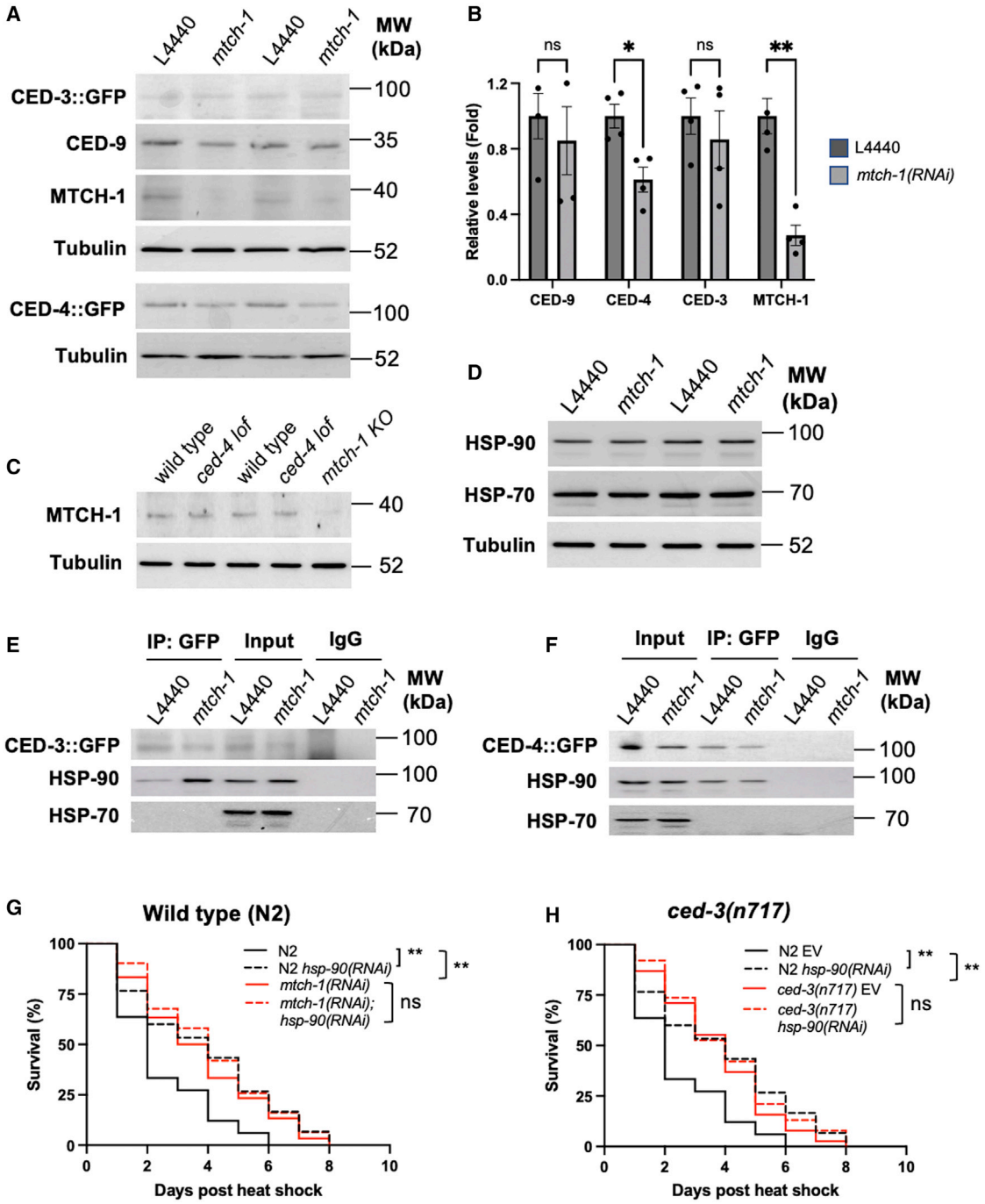

Figure 6. Reduced MTCH-1 activity selectively induces heat shock response genes in reproductively active adults

(A and B) Representative images (A) and quantification (B) of CED-3::GFP, CED-4::GFP, CED-9, MTCH-1, and tubulin levels in day 3 adult EV (L4440) control or *mtch-1(RNAi)* worms. Values are the mean of at least 3 biological replicates.

(C) Representative images of MTCH-1 and tubulin levels in day 3 wild-type (N2), *ced-4(n1162)*, and *mtch-1(ok1800)* animals. At least 3 biological replicates were analyzed per group.

(D) Representative images of HSP-90, HSP-70, and tubulin levels in day 3 adult EV (L4440) control or *mtch-1(RNAi)* worms. At least 3 biological replicates were analyzed per group.

(E and F) Representative images of HSP-90 and HSP-70 after GFP or IgG IP from (E) CED-3::GFP or (F) CED-4::GFP animals. Experiments were performed three times.

(G and H) Survival of (G) wild-type (N2) and (H) *ced-3(n717)* animals on day 3 of adulthood following exposure to heat shock (35°C, 4 h). Worms were grown on EV control or *mtch-1(RNAi)*. Three independent trials were performed per stress resistance experiment.

All error bars denote SEM. Statistical significance was calculated using unpaired, two-tailed Student's t test (B) or the Mantel-Cox log rank test (G and H). ns, not significant; *p < 0.05 and **p < 0.01. Survival statistics for all trials related to (G) and (H) (including n values) can be found in Table S1. See also Figure S6.

other proteostasis modifying pathways, MTCH-1 knockdown does not maintain the activity of the HSR or UPR in reproductive adulthood. Instead, we find that *mtch-1(RNAi)* results in the increased basal expression of multiple HSF-1 target genes, including HSP-16, HSP-70, DNJ-19, and CCT-1. Among the chaperones induced by *mtch-1(RNAi)*, elevated levels of small heat shock proteins are associated with increased longevity and suppression of age-related protein aggregation.[11,17] However, increased levels of small heat shock proteins have also been shown to promote protein aggregation in post-reproductive tissues.[42] It is likely that the differential effects of sHSPs on age-related protein aggregation are due to differences in substrate interactions, the cellular environment, and differences in the composition of the PN.

Our data suggest that reduced MTCH-1 levels may increase HSF-1 activity by titrating HSP-90 away from HSF-1-repressive complexes and toward CED-3. It has previously been shown that inhibiting HSP-90 activity in adulthood, either genetically or pharmacologically, can activate HSF-1 and extend lifespan in *C. elegans* and can suppress polyglutamine aggregation and toxicity in fly and mouse models of neurodegenerative disease and kill senescent cells in mammals.[32,43–46] Future studies to fully understand how the interplay between HSP-90 and PCD factors derepresses HSF-1 activity, and to determine how HSP-90 inhibition exerts its beneficial effects on long-term tissue health, will be crucial.

Although we find that knockdown of *mtch-1* modestly extends median lifespan, neither *ced-3* or *ced-4* mutants are reported to be long lived.[35,47] Given that reduced MTCH-1 activity acts through inhibition of CED-3/4 to maintain proteostasis, and that inhibition of CED-3/4 alone enhances stress resistance in adult animals, it is clear that maintenance of proteostasis capacity and elevated stress resistance do not always translate to an increased lifespan. A similar phenomenon has also been observed in eggshell compromised *cbd-1* mutants,[16] which increase HSF-1 activity and suppress polyglutamine aggregation but are not long lived. It is possible that the presence or absence of effects on lifespan by proteostasis modifying interventions reflects the extent to which different tissue-specific pathologies, many of which may be caused by the drive to rapidly reproduce, are altered.[48]

Finally, the fact that MTCH-1 controls HSF-1 activity and proteostasis capacity independently of previously reported pathways begs a very important question: why are there so many mechanisms for altering the long-term activity of HSF-1? Although we do not currently know the answer to this, we speculate that this may reflect the fact that HSF-1 activity is integrated into a complex network of pathways that couple nutritional status, reproductive potential and pathogenicity of the environment, with long-term proteostasis capacity. Therefore, the presence of multiple pathways regulating HSF-1 activity may allow organisms to tailor HSF-1 activity and PN composition to meet a diverse range of challenges sensed. It is plausible that such an approach would be far more efficient than the broad activation of HSF-1 by a single pathway. Future attempts to understand why increased HSF-1 activity promotes longevity in some contexts but not others, and understanding precisely how reduced MTCH-1 activity, GSC removal, and ETC impairment specifically alter HSF-1 activity and proteome composition, will be key to developing a complete picture of the relationship between HSF-1, proteostasis capacity and aging.

Limitations of the study

One conceptual limitation of this study is that we have not shown that a shift in HSP-90-HSF-1 binding is the sole driver of increased PN gene expression in response to MTCH-1 perturbation. Although this is a plausible model, it remains possible that alterations in other HSP-90 client interactions indirectly lead to enhanced HSF-1 activity and elevated expression of PN genes. A more comprehensive, unbiased assessment of HSP-90 client interactions under control and *mtch-1(RNAi)* conditions, may allow us to address this. In addition, there are some technical limitations to the study. One is that GFP tagged CED-3 and CED-4 proteins were used to study HSP-90 interactions as antibodies against CED-3 and CED-4 are not readily available. Furthermore, although we were able to perform experiments using mutants with an inactive PCD pathway, we were unable to perform reciprocal experiments with animals in which the PCD pathway is constitutively active, as these mutants do not develop.[25]

STAR★METHODS

Detailed methods are provided in the online version of this paper and include the following:

- KEY RESOURCES TABLE
- RESOURCE AVAILABILITY
  - Lead contact
  - Materials availability
  - Data and code availability
- EXPERIMENTAL MODEL AND SUBJECT DETAILS
  - C. elegans strains and culture conditions
- METHOD DETAILS
  - RNA interference
  - Lifespan and stress resistance assays
  - Proteostasis sensor assays
  - RNA extraction, cDNA synthesis and RTqPCR
  - RNA-sequencing and analysis
  - Apoptosis assays
  - TMRE staining
  - Oil Red O staining
  - ATP assays
  - Protein extraction and western blotting
  - Protein extraction and immunoprecipitation
  - Chromatin immunoprecipitation
  - Oxygen consumption assays
  - Mitochondrial morphology assays
- QUANTIFICATION AND STATISTICAL ANALYSIS

SUPPLEMENTAL INFORMATION

Supplemental information can be found online at https://doi.org/10.1016/j.celrep.2022.111690.

ACKNOWLEDGEMENTS

We would like to thank all members of the Labbadia lab as well as David Gems, Barbara Conradt, Zheng Zhou, Rahul Samant, and Rick Morimoto for helpful

discussions around the work and the generous sharing of strains, reagents, protocols and equipment. We would also like to thank the University College London (UCL) Biosciences Microscopy suite and the Institute of Healthy Ageing for access to confocal and fluorescence microscopes, Janine Kirstein for sharing muscle and neuronal ABeta strains, Patricija van Oosten Hawle for sharing the HSP-90 antibody with us, the Caenorhabditis Genetics Center (CGC) for providing strains used in this study, and Novogene UK for carrying out RNA sequencing. This work was funded by a BBSRC David Phillips Fellowship (BB/P005535/1) awarded to J.L.

AUTHOR CONTRIBUTIONS

Conceptualization, J.L.; methodology, J.L., Y.A., A.P.E., and N.T.-P.; software, R. Wellman; validation, J.L., Y.A., A.P.E., and N.T.-P.; formal analysis, J.L., Y.A., A.P.E., and N.T.-P.; investigation, J.L., Y.A., A.P.E., N.T.-P., H.C., R. Wellman, and R. Williams; resources, J.L.; data curation, J.L. and R. Wellman; writing – original draft, J.L., writing – review & editing, J.L., Y.A., A.P.E., N.T.-P., H.C., R. Wellman, and R. Williams; visualization, J.L., Y.A., A.P.E., N.T.-P., H.C., and R. Wellman; supervision, J.L., project administration, J.L.; funding acquisition, J.L.

DECLARATION OF INTERESTS

The authors declare no competing interests.

INCLUSION AND DIVERSITY

We support inclusive, diverse, and equitable conduct of research.

Received: January 10, 2022
Revised: September 12, 2022
Accepted: October 28, 2022
Published: November 22, 2022

REFERENCES

1. Labbadia, J., and Morimoto, R.I. (2015). The biology of proteostasis in aging and disease. Annu. Rev. Biochem. *84*, 435–464.
2. Hipp, M.S., Kasturi, P., and Hartl, F.U. (2019). The proteostasis network and its decline in ageing. Nat. Rev. Mol. Cell Biol. *20*, 421–435.
3. Chiti, F., and Dobson, C.M. (2017). Protein misfolding, amyloid formation and human disease: a summary of progress over the last decade. Annu. Rev. Biochem. *86*, 27–68.
4. Ben-Zvi, A., Miller, E.A., and Morimoto, R.I. (2009). Collapse of proteostasis represents an early molecular event in Caenorhabditis elegans aging. Proc. Natl. Acad. Sci. USA *106*, 14914–14919.
5. Blumenstock, S., Schulz-Trieglaff, E.K., Voelkl, K., Bolender, A.L., Lapios, P., Lindner, J., Hipp, M.S., Hartl, F.U., Klein, R., and Dudanova, I. (2021). Fluc-EGFP reporter mice reveal differential alterations of neuronal proteostasis in aging and disease. EMBO J. *40*, e107260.
6. David, D.C., Ollikainen, N., Trinidad, J.C., Cary, M.P., Burlingame, A.L., and Kenyon, C. (2010). Widespread protein aggregation as an inherent part of aging in C. elegans. P Biol. *8*, e1000450.
7. Demontis, F., and Perrimon, N. (2010). FOXO/4E-BP signaling in Drosophila muscles regulates organism-wide proteostasis during aging. Cell *143*, 813–825.
8. Labbadia, J., and Morimoto, R.I. (2015). Repression of the heat shock response is a programmed event at the onset of reproduction. Mol. Cell *59*, 639–650.
9. Shemesh, N., Shai, N., and Ben-Zvi, A. (2013). Germline stem cell arrest inhibits the collapse of somatic proteostasis early in Caenorhabditis elegans adulthood. Aging Cell *12*, 814–822.
10. Baird, N.A., Douglas, P.M., Simic, M.S., Grant, A.R., Moresco, J.J., Wolff, S.C., Yates, J.R., 3rd, Manning, G., and Dillin, A. (2014). HSF-1-mediated cytoskeletal integrity determines thermotolerance and life span. Science *346*, 360–363.
11. Hsu, A.L., Murphy, C.T., and Kenyon, C. (2003). Regulation of aging and age-related disease by DAF-16 and heat-shock factor. Science *300*, 1142–1145.
12. Kumsta, C., Chang, J.T., Schmalz, J., and Hansen, M. (2017). Hormetic heat stress and HSF-1 induce autophagy to improve survival and proteostasis in C. elegans. Nat. Commun. *8*, 14337.
13. Morley, J.F., and Morimoto, R.I. (2004). Regulation of longevity in Caenorhabditis elegans by heat shock factor and molecular chaperones. Mol. Biol. Cell *15*, 657–664.
14. Labbadia, J., Brielmann, R.M., Neto, M.F., Lin, Y.F., Haynes, C.M., and Morimoto, R.I. (2017). Mitochondrial stress restores the heat shock response and prevents proteostasis collapse during aging. Cell Rep. *21*, 1481–1494.
15. Shpigel, N., Shemesh, N., Kishner, M., and Ben-Zvi, A. (2019). Dietary restriction and gonadal signaling differentially regulate post-development quality control functions in Caenorhabditis elegans. Aging Cell *18*, e12891.
16. Sala, A.J., Bott, L.C., Brielmann, R.M., and Morimoto, R.I. (2020). Embryo integrity regulates maternal proteostasis and stress resilience. Genes Dev. *34*, 678–687.
17. Williams, R., Laskovs, M., Williams, R.I., Mahadevan, A., and Labbadia, J. (2020). A mitochondrial stress-specific form of HSF1 protects against age-related proteostasis collapse. Dev. Cell *54*, 758–772.e5.
18. Taylor, R.C., and Dillin, A. (2013). XBP-1 is a cell-nonautonomous regulator of stress resistance and longevity. Cell *153*, 1435–1447.
19. Morley, J.F., Brignull, H.R., Weyers, J.J., and Morimoto, R.I. (2002). The threshold for polyglutamine-expansion protein aggregation and cellular toxicity is dynamic and influenced by aging in Caenorhabditis elegans. Proc. Natl. Acad. Sci. USA *99*, 10417–10422.
20. Mohri-Shiomi, A., and Garsin, D.A. (2008). Insulin signaling and the heat shock response modulate protein homeostasis in the Caenorhabditis elegans intestine during infection. J. Biol. Chem. *283*, 194–201.
21. Brignull, H.R., Moore, F.E., Tang, S.J., and Morimoto, R.I. (2006). Polyglutamine proteins at the pathogenic threshold display neuron-specific aggregation in a pan-neuronal Caenorhabditis elegans model. J. Neurosci. *26*, 7597–7606.
22. Gallrein, C., Iburg, M., Michelberger, T., Koçak, A., Puchkov, D., Liu, F., Ayala Mariscal, S.M., Nayak, T., Kaminski Schierle, G.S., and Kirstein, J. (2021). Novel amyloid-beta pathology C. elegans model reveals distinct neurons as seeds of pathogenicity. Prog. Neurobiol. *198*, 101907.
23. Raemy, E., Montessuit, S., Pierredon, S., van Kampen, A.H., Vaz, F.M., and Martinou, J.C. (2016). Cardiolipin or MTCH2 can serve as tBID receptors during apoptosis. Cell Death Differ. *23*, 1165–1174.
24. Rottiers, V., Francisco, A., Platov, M., Zaltsman, Y., Ruggiero, A., Lee, S.S., Gross, A., and Libert, S. (2017). MTCH2 is a conserved regulator of lipid homeostasis. Obesity (Silver Spring) *25*, 616–625.
25. Conradt, B., and Xue, D. (2005). Programmed Cell Death (WormBook), pp. 1–13.
26. Yan, B., Memar, N., Gallinger, J., and Conradt, B. (2013). Coordination of cell proliferation and cell fate determination by CES-1 snail. PLoS Genet. *9*, e1003884.
27. Zhou, Z., Hartwieg, E., and Horvitz, H.R. (2001). CED-1 is a transmembrane receptor that mediates cell corpse engulfment in C. elegans. Cell *104*, 43–56.
28. Shaham, S., Reddien, P.W., Davies, B., and Horvitz, H.R. (1999). Mutational analysis of the Caenorhabditis elegans cell death gene ced-3. Genetics. Genetics *153*, 1655–1671.
29. Chen, F., Hersh, B.M., Conradt, B., Zhou, Z., Riemer, D., Gruenbaum, Y., and Horvitz, H.R. (2000). Translocation of C. elegans CED-4 to nuclear membranes during programmed cell death. Science *287*, 1485–1489.

30. Geng, X., Shi, Y., Nakagawa, A., Yoshina, S., Mitani, S., Shi, Y., and Xue, D. (2008). Inhibition of CED-3 zymogen activation and apoptosis in Caenorhabditis elegans by caspase homolog CSP-3. Nat. Struct. Mol. Biol. *15*, 1094–1101.

31. Harders, R.H., Morthorst, T.H., Lande, A.D., Hesselager, M.O., Mandrup, O.A., Bendixen, E., Stensballe, A., and Olsen, A. (2018). Dynein links engulfment and execution of apoptosis via CED-4/Apaf1 in C. elegans. Cell Death Dis. *9*, 1012.

32. Guisbert, E., Czyz, D.M., Richter, K., McMullen, P.D., and Morimoto, R.I. (2013). Identification of a tissue-selective heat shock response regulatory network. PLoS Genet *9*, e1003466.

33. Pandey, P., Saleh, A., Nakazawa, A., Kumar, S., Srinivasula, S.M., Kumar, V., Weichselbaum, R., Nalin, C., Alnemri, E.S., Kufe, D., and Kharbanda, S. (2000). Negative regulation of cytochomre-c mediated oligomerization of Apaf-1 and activation of procaspase-9 by heat shock protein 90. EMBO J. *19*, 4310–4322.

34. Judy, M.E., Nakamura, A., Huang, A., Grant, H., McCurdy, H., Weiberth, K.F., Gao, F., Coppola, G., Kenyon, C., and Kao, A.W. (2013). A shift to organismal stress resistance in programmed cell death mutants. PLoS Genet. *9*, e1003714.

35. Yee, C., Yang, W., and Hekimi, S. (2014). The intrinsic apoptosis pathway mediates the pro-longevity response to mitochondrial ROS in C. elegans. Cell *157*, 897–909.

36. Weaver, B.P., Weaver, Y.M., Omi, S., Yuan, W., Ewbank, J.J., and Han, M. (2020). Non-canonical caspase activity antagonizes p38 MAPK stress-priming function to support development. Dev. Cell *53*, 358–369.e6.

37. Rolland, S.G., Schneid, S., Schwarz, M., Rackles, E., Fischer, C., Haeussler, S., Regmi, S.G., Yeroslaviz, A., Habermann, B., Mokranjac, D., et al. (2019). Compromised mitochondrial protein import acts as a signal for UPR(mt). Cell Rep. *28*, 1659–1669.e5.

38. Curran, S.P., and Ruvkun, G. (2007). Lifespan regulation by evolutionarily conserved genes essential for viability. PLoS Genet. *3*, e56.

39. Karch, C.M., Ezerskiy, L.A., Bertelsen, S., and Alzheimer's Disease Genetics Consortium ADGC; and Goate, A.M. (2016). Alzheimer's disease risk polymorphisms regulate gene expression in the ZCWPW1 and the CELF1 loci. PLoS One *11*, e0148717.

40. Silva, M.C., Fox, S., Beam, M., Thakkar, H., Amaral, M.D., and Morimoto, R.I. (2011). A genetic screening strategy identifies novel regulators of the proteostasis network. PLoS Genet. *7*, e1002438.

41. Kawasaki, F., Koonce, N.L., Guo, L., Fatima, S., Qiu, C., Moon, M.T., Zheng, Y., and Ordway, R.W. (2016). Small heat shock proteins mediate cell-autonomous and -nonautonomous protection in a Drosophila model for environmental-stress-induced degeneration. Dis. Model. Mech. *9*, 953–964.

42. Walther, D.M., Kasturi, P., Zheng, M., Pinkert, S., Vecchi, G., Ciryam, P., Morimoto, R.I., Dobson, C.M., Vendruscolo, M., Mann, M., and Hartl, F.U. (2015). Widespread proteome remodeling and aggregation in aging C. elegans. Cell *161*, 919–932.

43. Waza, M., Adachi, H., Katsuno, M., Minamiyama, M., Sang, C., Tanaka, F., Inukai, A., Doyu, M., and Sobue, G. (2005). 17-AAG, an Hsp90 inhibitor, ameliorates polyglutamine-mediated motor neuron degeneration. Nat. Med. *11*, 1088–1095.

44. Fujikake, N., Nagai, Y., Popiel, H.A., Okamoto, Y., Yamaguchi, M., and Toda, T. (2008). Heat shock transcription factor-1 activating compounds suppress polyglutamine-induced neurodegeneration through induction of multiple molecular chaperones. J. Biol. Chem. *283*, 26188–26197.

45. Fuhrmann-Stroissnigg, H., Ling, Y.Y., Zhao, J., McGowan, S.J., Zhu, Y., Brooks, R.W., Grassi, D., Gregg, S.Q., Stripay, J.L., Dorronsoro, A., et al. (2017). Identification of HSP90 inhibitors as a novel class of senolytics. Nat. Commun. *8*, 422.

46. Fuentealba, M., Dönertaş, H.M., Williams, R., Labbadia, J., Thornton, J.M., and Partridge, L. (2019). Using the drug-protein interactome to identify anti-ageing compounds for humans. Plos Comput. Biol. *15*, e1006639.

47. de la Guardia, Y., Gilliat, A.F., Hellberg, J., Rennert, P., Cabreiro, F., and Gems, D. (2016). Run-on of germline apoptosis promotes gonad senescence in C. elegans. Oncotarget *7*, 39082–39096.

48. Gems, D., Kern, C.C., Nour, J., and Ezcurra, M. (2021). Reproductive suicide: similar mechanisms of aging in C. elegans and pacific salmon. Front. Cell Dev. Biol. *9*, 688788.

49. Van Oosten-Hawle, P., Porter, R.S., and Morimoto, R.I. (2013). Regulation of organismal proteostasis by transcellular chaperone signalling. Cell *153*, 1366–1378.

50. Rolland, S.G., Lu, Y., David, C.N., and Conradt, B. (2009). The BCL-2-like protein CED-9 of C. elegans promotes FZO-1, Mfn1, 2- and EAT-3/Opa1-dependent mitochondrial fusion. J. Cell Biol. *186*, 525–540.

51. Sherrard, R., Luehr, S., Holzkamp, H., McJunkin, K., Memar, N., and Conradt, B. (2017). miRNAs cooperate in apoptosis regulation during *C. elegans* development. Genes Dev. *31*, 209–222.

52. Prahlad, V., and Morimoto, R.I. (2011). Neuronal circuitry regulates the response of Caenorhabditis elegans to misfolded proteins. Proc. Natl. Acad. Sci. USA *108*, 14204–14209.

53. Li, J., Chauve, L., Phelps, G., Brielmann, R.M., and Morimoto, R.I. (2016). E2F coregulates an essential HSF developmental program that is distinct from the heat-shock response. Genes Dev. *30*, 2062–2075.

54. Schindelin, J., Arganda-Carreras, I., Frise, E., Kaynig, V., Longair, M., Pietzsch, T., Preibisch, S., Rueden, C., Saalfeld, S., Schmid, B., et al. (2012). Fiji: an open-source platform for biological-image analysis. Nat. Methods *9*, 676–682.

55. Raudvere, U., Kolberg, L., Kuzmin, I., Arak, T., Adler, P., Peterson, H., and Vilo, J. (2019). G:Profiler: a web server for functional enrichment analysis and conversions of gene lists (2019 update). Nucleic Acids Res. *47*, W191–W198.

56. Love, M.I., Huber, W., and Anders, S. (2014). Moderated estimation of fold change and dispersion for RNA-seq data with DESeq2. Genome Biol. *15*, 550.

57. Brenner, S. (1974). The genetics of Caenorhabditis elegans. Genetics *77*, 71–94.

58. Kamath, R.S., Fraser, A.G., Dong, Y., Poulin, G., Durbin, R., Gotta, M., Kanapin, A., Le Bot, N., Moreno, S., Sohrmann, M., et al. (2003). Systematic functional analysis of the Caenorhabditis elegans genome using RNAi. Nature *421*, 231–237.

59. Margie, O., Palmer, C., and Chin-Sang, I. (2013). C. elegans chemotaxis assay. J. Vis. Exp.e50069

60. Wählby, C., Conery, A.L., Bray, M.A., Kamentsky, L., Larkins-Ford, J., Sokolnicki, K.L., Veneskey, M., Michaels, K., Carpenter, A.E., and O'Rourke, E.J. (2014). High- and low-throughput scoring of fat mass and body fat distribution in C. elegans. Methods *68*, 492–499.

61. Koopman, M., Michels, H., Dancy, B.M., Kamble, R., Mouchiroud, L., Auwerx, J., Nollen, E.A.A., and Houtkooper, R.H. (2016). A screening-based platform for the assessment of cellular respiration in Caenorhabditis elegans. Nat. Protoc. *11*, 1798–1816.

STAR★METHODS

KEY RESOURCES TABLE

REAGENT or RESOURCE	SOURCE	IDENTIFIER
Antibodies		
Mouse monoclonal anti-GFP (mixture of clones 13.1 and 7.1)	Sigma	Cat# 11814460001 (Roche); RRID: AB_390913
Mouse monoclonal anti-GFP (JL8)	Clontech	Cat# 632380 (Takara Bio); RRID: AB_10013427
Mouse monoclonal anti-alpha tubulin	Sigma	Cat# T5168, B512; RRID: AB_477579
Rabbit polyclonal anti HSP-90	Gift from Dr Patricija van Oosten-Hawle (van Oosten Hawle et al.[49])	N/A
Rabbit polyclonal anti CED-9	Gift from Prof. Barbara Conradt (Rolland et al.[50])	N/A
Rabbit polyclonal anti MTCH1	Invitrogen	Cat# PA5-42964; RRID: AB_2576880
Bacterial and virus strains		
E. coli OP50	CGC	WB OP50; RRID: WB-STRAIN:OP50
E. coli HT115	CGC	WB HT115; RRID: WB-STRAIN:HT115
Chemicals, peptides, and recombinant proteins		
Paraquat	Sigma	Cat# 856177
Tunicamycin	Cambridge Bioscience	Cat# 11445
Benzaldehyde	Sigma	Cat# B1334
Critical commercial assays		
ATP assay Kit	Sigma	Cat# MAK135
Tetramethylrhodamine, Ethyl Ester, Perchlorate (TMRE)	Invitrogen	Cat# T669
Oil Red O	Merck	Cat# 102419
iScript cDNA synthesis kit	BioRad	Cat# 1708890
Seahorse FluxPaks	Agilent	Lot# W06322
Deposited data		
N2 – D3 adults - EV v mtch-1(RNAi) RNAseq data	This study	GEO: GSE195594
Experimental models: Organisms/strains		
C. elegans: Strain N2 Bristol	Caenorhabditis Genetics Center	RRID: WB-STRAIN: WBStrain00000001
C. elegans: Strain VC1345 *mtch-1(ok1800)/ mIn1[mIs14 dpy-10(e128) II]*	Caenorhabditis Genetics Center	RRID: WB-STRAIN: WBStrain00036531
C. elegans: Strain MT4770 *ced-9(n1950) III*	Caenorhabditis Genetics Center	RRID: WB-STRAIN: WBStrain00027154
C. elegans: Strain MT2547 *ced-4(n1162) III*	Caenorhabditis Genetics Center	RRID: WB-STRAIN: WBStrain00026975
C. elegans: Strain MT1522 *ced-3(n717) IV*	Caenorhabditis Genetics Center	RRID: WB-STRAIN: WBStrain00026860
C. elegans: Strain MD131 *egl-1(n3330) IV*	Gift from Prof. Barbara Conradt (Sherrard et al.[51])	N/A
C. elegans: Strain BXN723 *fzo-1(cjn20) II*	Caenorhabditis Genetics Center	N/A
C. elegans: Strain CU6372 *drp-1(tm1108) IV*	Caenorhabditis Genetics Center	RRID: WB-STRAIN: WBStrain00005196
C. elegans: Strain SJ4100 *zcIs13 [hsp-6p::gfp + lin-15(+)] V*	Caenorhabditis Genetics Center	RRID: WB-STRAIN: WBStrain00034068
C. elegans: Strain AD1116 *eat-2(ad1116) II*	Caenorhabditis Genetics Center	RRID: WB-STRAIN: WBStrain00005548
C. elegans: Strain CF1903 *glp-1(e2144ts) III*	Caenorhabditis Genetics Center	RRID: WB-STRAIN: WBStrain00004531
C. elegans: Strain MQ989 *isp-1(qm150);ctb-1(qm189)*	Caenorhabditis Genetics Center	RRID: WB-STRAIN: WBStrain00026672

(*Continued on next page*)

Continued

REAGENT or RESOURCE	SOURCE	IDENTIFIER
C. elegans: Strain MD701 *bcIs39 [lim-7p::ced-1::gfp + lin-15(+) V*	Caenorhabditis Genetics Center	RRID: WB-STRAIN: WBStrain00026469
C. elegans: Strain *bcIs66[tph-1p:: his-24::gfp] III*	Gift from Prof. Barbara Conradt (Yan et al.[26])	N/A
C. elegans: Strain AM738 *rmIs297[vha-6p::Q40::YFP + rol-6(su1006)]*	Gift from Prof. Rick Morimoto (Prahlad and Morimoto[52])	N/A
C. elegans: Strain AM140 *rmIs132[unc-54p::Q35::YFP]*	Caenorhabditis Genetics Center	RRID: WB-STRAIN: WBStrain00000182
C. elegans: Strain AM101 *rmIs110 [F25B3.3p::Q40::YFP]*	Caenorhabditis Genetics Center	RRID: WB-STRAIN: WBStrain00000178
C. elegans: Strain CB1301 *unc-54 (e1301ts) I*	Caenorhabditis Genetics Center	RRID: WB-STRAIN: WBStrain00004294
C. elegans: Strain PS351 *hsf-1(sy441) I*	Caenorhabditis Genetics Center	RRID: WB-STRAIN: WBStrain00030901
C. elegans: Strain AM1061 *rmSi1[hsf-1p(4Kb)::hsf-1(minigene)::gfp::3′UTR hsf-1 + Cbr unc-119(+) II; hsf-1(ok600)]*	Gift from Prof. Rick Morimoto (Li et al.[53])	N/A
C. elegans: Strain CF1038 *daf-16(mu86) I*	Caenorhabditis Genetics Center	RRID: WB-STRAIN: WBStrain00004840
C. elegans: Strain JKM2 *Is* [*rgef1* p::SignalpeptideAbeta (1–42)::*hsp3* (IRES)::wrm ScarletAbeta(1–42):: *unc54* (3′UTR) + *rps 0*p::HygroR]	Gift from Prof. Janine Kirstein (Gallrein et al.[22])	N/A
C. elegans: Strain JKM3 *Is* [*rgef-1*p::wrmScarlet::*unc-54*(3′UTR) + *rps-0*p::HygroR]	Gift from Prof. Janine Kirstein (Gallrein et al.[22])	N/A
C. elegans: Strain JKM7 *Is* [*myo-3*p::Signalpeptide-Abeta (1–42)::*hsp-3* (IRES)::wrm Scarlet-Abeta(1–42)::*unc-54*(3′UTR) + *rps -0*p::HygroR]	Gift from Prof. Janine Kirstein (Gallrein et al.[22])	N/A
C. elegans: Strain JKM8 *Ex* [*myo-3*p::wrmScarlet-Abeta:: *unc-54*(3′UTR) + *rps-0*p::HygroR]	Gift from Prof. Janine Kirstein (Gallrein et al.[22])	N/A
C. elegans: Strain SJ4103 *zcIs14 [myo-3::GFP(mit)]*	Caenorhabditis Genetics Center	RRID: WB-STRAIN: WBStrain00034069
C. elegans: Strain XR6 *lagr-1(gk327); opIs219[ced-4p::ced-4::gfp]*	Caenorhabditis Genetics Center	RRID: WB-STRAIN: WBStrain00040675
C. elegans: Strain CU394 *smIs10 [ced-3p::ced-3::gfp + rol-6(su1006)] I*	Caenorhabditis Genetics Center	RRID: WB-STRAIN: WBStrain00005189
Oligonucleotides		
Please see Table S2 for a complete list of primers used in this study	N/A	N/A
Software and algorithms		
FIJI	Schindelin et al.[54]	https://imagej.net/Fiji#Downloads
gProfiler	Raudvere et al.[55]	https://biit.cs.ut.ee/gprofiler/page/faq
DESeq2	Love, Huber, and Anders[56]	https://bioconductor.org/packages/release/bioc/html/DESeq2.html

RESOURCE AVAILABILITY

Lead contact

Further information and requests for resources and reagents should be directed to and will be fulfilled by the lead contact, John Labbadia (j.labbadia@ucl.ac.uk).

Materials availability

This study did not generate new, unique reagents.

Data and code availability

- RNA-seq data have been deposited at GEO and are publicly available as of the date of publication. Accession numbers are listed in the key resources table.
- This paper does not report original code.
- Any additional information required to re-analyze the data reported in this paper is available from the lead contact upon request.

EXPERIMENTAL MODEL AND SUBJECT DETAILS

C. elegans strains and culture conditions

All strains were maintained at 20°C on NGM plates seeded with *Eschericia coli* OP50 using standard husbandry techniques as previously described.[57] Populations of age-synchronised animals were obtained through a 1 hour period of egg-laying onto seeded plates. Strains used in this study were: N2 Bristol (wild type laboratory strain), VC1345 *mtch-1(ok1800),* MT4770 *ced-9(n1950)*, MT2547 *ced-4(n1162)*, MT1522 *ced-3(n717)*, MD131 *egl-1(n3330)*, BXN723 *fzo-1(cjn20)*, CU6372 *drp-1(tm1108)*, SJ4100 (zcIs13 [*hsp-6*p::gfp + lin-15(+)], AD1116 *eat-2(ad1116)*, CF1903 *glp-1(e2144ts)*, MQ989 *isp-1(qm150);ctb-1(qm189)*, MD701 (bcIs39 [*lim-7*p::*ced-1*::gfp + lin-15(+)], bcIs66[*tph-1*p::*his-24*::gfp], AM738 (rmIs297 [*vha-6*p::Q(44)::YFP, *rol-6(su1006)*]), AM140 (rmIs132 [*unc-54*p::Q(35)::YFP]), AM101 (rmIs110 [*F25B3.3*p::Q(40)::YFP]), CB1301 *unc-54(e1301ts)*, PS3551 *hsf-1(sy441),* CF1038 *daf-16(mu86),* JKM2 (*Is* [*rgef1*p::SignalpeptideAbeta (1−42)::*hsp3* (IRES)::wrm ScarletAbeta(1−42)::*unc54* (3'UTR) + *rps 0*p::HygroR]), JKM3 (*Is* [*rgef-1*p::wrmScarlet::*unc-54*(3′UTR) + *rps-0*p::HygroR]), JKM7 (*Is* [*myo-3*p::Signalpeptide-Abeta(1−42)::*hsp-3* (IRES)::wrm Scarlet-Abeta(1−42)::*unc-54*(3′UTR) + *rps -0*p::HygroR]), JKM8 (*Ex* [*myo-3*p::wrmScarlet-Abeta::*unc-54*(3′UTR) + *rps-0*p::HygroR]), SJ4103 zcIs14 [myo-3::GFP(mit)], AM1061 (rmSi1[*hsf-1*p(4Kb::*hsf-1*(minigene)::gfp::3′UTR *hsf-1* + Cbr *unc-119(+)]*; *hsf-1(ok600)*), XR6 (opIs219[*ced-4*p::*ced-4*::gfp]), and CU394 (*ced-3*p::*ced-3*::gfp + *rol-6(su1006)*]).

METHOD DETAILS

RNA interference

All clones were sequenced verified before use and were obtained from the Ahringer RNAi library.[58] RNAi was performed by growing bacteria for 16 hours at 37°C in LB containing 100 ug/ml ampicillin, with shaking (220 rpm). Cultures were then induced with 5 mM IPTG and allowed to grow at 37°C for a further 3 hours. Following induction, bacteria were allowed to cool at room temperature and were then seeded onto NGM plates containing 100 ug/ml ampicillin and 1 mM IPTG. Seeded plates were allowed to dry at room temperature before use.

Lifespan and stress resistance assays

In all lifespan and stress resistance assays, survival was scored by gently touching worms with a platinum pick at indicated time points. Worms were scored as dead in the absence of touch response and absence of pharyngeal pumping. In lifespan assays, worms exhibiting intestinal prolapse through the vulva (rupturing) or internal hatching of progeny (bagging) were censored. For thermorecovery assays, worms were heat shocked on seeded NGM plates at 33°C for 4 hours and allowed to recover at 20°C. For tunicamycin or paraquat treatment, worms were transferred to seeded NGM plates containing tunicamycin (50 ug/ml) or paraquat (10 mM) on day 1 or day 3 of adulthood and maintained at 20°C. Survival statistics for all experimental repeats can be found in Table S1.

Proteostasis sensor assays

Polyglutamine aggregation was scored in muscle and intestinal proteostasis sensors at indicated time points under a Nikon SMZ1270 fluorescence dissecting stereomicroscope. Aggregates were determined to be any discrete foci exhibiting fluorescence signal above the background diffuse signal. Representative images of worms immobilised on 3% agar pads in 3 mM levamisole were captured using a Zeiss Imager.Z2 microscope and Hamamatsu ORCA-Flash 4.0 digital CMOS camera.

Muscle function was assessed in polyglutamine, Amyloid Beta and metastable myosin expressing animals by scoring paralysis at different days of adulthood. Animals were scored as paralysed when they were unable to move forwards or backwards at least one body length in response to touch with a platinum pick.

Neuronal function was assessed through benzaldehyde-based chemotaxis assays as previously described.[59] Chemotaxis plates were divided into 4 equal quadrants around a central circle measuring 1 cm in diameter. 1% benzaldehyde or water mixed in equal volumes with 0.5M sodium azide were spotted within adjacent quadrants, 2 cm from the origin circle and an equal distance from one another. Age-synchronized animals were washed 5 times in M9 buffer, added directly to the centre of the origin circle and placed at 20°C for 60 minutes. Chemotaxis was scored immediately after by counting the number of worms in each quadrant. The chemotaxis

index for each treatment group was calculated by subtracting the number of worms in control quadrants from the number of worms in test quadrants and dividing the result by the total number of worms scored.

RNA extraction, cDNA synthesis and RTqPCR

Approximately 100–200 adult animals per treatment group were lysed in 250 μl of Trizol by vortexing for 20 minutes at 4°C. RNA was purified using an RNeasy extraction kit as per manufacturer's instructions. cDNA was generated using 1 ug of total RNA and an iScript cDNA synthesis kit. Real-time quantitative PCR was performed using a Biorad CFX96 Real-time PCR detection system and BioRad SsoAdvanced SYBR green super mix. Expression of genes of interest was calculated relative to the housekeeping genes *rpb-2* and *cdc-42* using the standard curve method. Sequences for all primer pairs used in this study can be found in Table S2.

RNA-sequencing and analysis

RNA integrity was assessed using an RNA Nano 6000 assay kit and an Agilent Bioanalyzer 2100 system. Following this, mRNA was purified from 1 μg of total RNA using poly-dT magnetic beads and cDNA libraries were generated using random hexamers and M-MuLV reverse transcriptase for first strand synthesis, followed by second strand synthesis using DNA polymerase I and RNase H. Fragments were blunt-ended and adapters were ligated before PCR was performed using Phusion high fidelity DNA polymerase. PCR products were purified using an AMPure XP system and library quality was checked using an Agilent Bioanalyzer 2100. Libraries were sequenced using an Illumina Novaseq 6000 platform to generate paired-end 150 base pair reads at a depth of 20 million reads per sample. Following sequencing, raw data was checked and reads containing adapter sequences, poly-N reads or poor-quality sequences were removed. Reads were then aligned to the *C. elegans* reference genome using Hisat2 v2.0.5 and featureCounts v1.5.0-p3 was used to quantify the number of reads mapped to each gene. Differential expression testing was carried out using DE-Seq2 and p-values were adjusted using Benjamini-Hochberg. Z-scores were calculated for each gene from log FPKM expression data for all differentially expressed genes (> 1.5-fold, adj $p < 0.05$) or UPR genes of interest and was plotted using the ComplexHeatmap function in R. Samples were then clustered using unsupervised hierarchical clustering by the Ward D2 method. Up or down regulated genes were analysed using the g:profiler tool to identify KEGG processes/pathways and Gene Ontology categories that were enriched in either group.

Apoptosis assays

Cell death was scored in NSM neurons by manually counting the number of HIS-24::GFP positive cells present on day 1 of adulthood under a Nikon SMZ1270 fluorescence dissecting stereomicroscope. Cell death in the germline was scored by mounting CED-1::GFP expressing animals on 3% agarose pads in 3 mM levamisole and manually counting the number of CED-1::GFP halos present in each gonad arm on day 3 of adulthood at 40X magnification using a Zeiss Imager.Z2 microscope.

TMRE staining

Animals at the desired age were grown at 20°C on plates (in the dark) in the presence of 150 nM tetramethylrhodamine, ethyl ester, perchlorate (TMRE) for 24 h. Stained worms were washed with M9 buffer (3g KH_2PO_4, 6g Na_2HPO_4, 5g NaCl, and 1 ml 1M $MgSO_4$ per litre H_2O) before being immobilized with 3mM levamisole and mounted on 3% agarose pads. Worms were imaged using a Zeiss Imager.Z2 microscope, with all images acquired under the same exposure settings. Average pixel intensity values were calculated by sampling images of different animals and the mean pixel intensity for each animal was calculated using ImageJ software.

Oil Red O staining

Staining for lipid levels was essentially performed as previously described.[60] Breifly, worms were washed 3 times in M9 buffer, fixed immediately in 60% isopropanol at room temperature, and then stained with freshly filtered ORO (60% ORO working solution) overnight at 25°C. Oil Red O solution was then washed-out using M9-0.01% Triton-X and worms were mounted on 3% agarose pads. Images were acquired on a Nikon SMZ1270 stereo microscope with a DS-Fi3 5.9 MP colour camera. Images were processed using ImageJ.

ATP assays

Approximately 500 wildtype N2 worms were cultured on plates with control and *mtch-1*(RNAi) and collected on Day 3 of adulthood. Worm pellets were resuspended in 50μl RIPA buffer lysate and protein concentration in each sample was estimated using the Pierce™ BCA Protein Assay Kit (Thermo Scientific) following the instructions of the manufacturer. ATP levels were quantified using a luciferin/luciferase-based ADP/ATP Ratio assay kit (Sigma Aldrich) as per manufacturer's instructions. Luminescence was then measured using a Tecan Infinite M200 microplate reader and levels of ATP were calculated.

Protein extraction and western blotting

To extract protein for western blotting, worms (approximately 500 – 1000) were collected in M9, pelleted, and then resuspended in RIPA buffer supplemented with a protease inhibitor cocktail tablet. Worm pellets were then flash frozen in liquid nitrogen and ground in microcentrifuge tubes using a plastic dounce homogenizer. Freezing and grinding were performed twice, and effectiveness of lysing was confirmed by checking a sample of the lysate under a dissecting microscope. Lysates were then centrifuged at

13,000 rpm at 4°C for 15 minutes and the supernatant was collected. Proteins were separated by SDS-PAGE and transferred to nitrocellulose membranes before probing with primary antibodies. Blots were incubated with primary antibodies for 1h at room temperature (HSP-90 - 1:5000, tubulin - 1:10,000) or overnight at 4°C (GFP - 1:1000, HSP-70 - 1:1000), washed three times with PBS-0.2% Tween, incubated with secondary antibodies for 1h at room temperature (mouse-HRP – 1:5000, rabbit-HRP – 1:5000), washed a further three times with PBS-0.2% Tween, and then developed using ECL detection reagents and an Amersham ImageQuant800 detection system. Densitometry of protein bands was performed using ImageJ gel analysis tools.

Protein extraction and immunoprecipitation

Protein lysates were obtained as described for western blotting with the exceptions that approximately 20,000 worms were harvested and lysed in modified RIPA buffer. Pulldowns were performed by incubating 2 mg of protein lysate with 20 ul of washed and pre-blocked Protein G Dynabeads, and 2 ug of antibody (GFP, CED-9 or normal IgG) in 500 ul of pulldown buffer, overnight at 4°C. Following incubation, beads were washed three times with modified RIPA buffer. For HSP-90 co-IPs, 0.025% SDS was added to the wash buffer to reduce background binding. After washing, beads were boiled at 95°C in 50 ul Laemmli buffer. SDS-PAGE and western blotting were then performed as described above.

Chromatin immunoprecipitation

Chromatin immunoprecipitation was performed as previously described.[14] Briefly, 20,000 worms were harvested in M9, pelleted and re-suspended in 1% formaldehyde-PBS to promote cross-linking. Worms were fixed for 30 minutes at room temperature, washed three times in PBS and then resuspended in FA buffer. Worms were then dounce homogenized on ice before being subjected to sonication using a Diagenode Bioruptor sonicator (15 rounds of 30s on 1 min off). Samples were then centrifuged at 4°C for 15 minutes and lysates were subjected to 5 more rounds of sonication to shear chromatin to approximately 500 bp in size. Pulldowns were performed by incubating 2 mg of pre-cleared chromatin with 20 ul of washed and pre-blocked Protein G Dynabeads and 2 ug antibody (anti-GFP) in 1 ml of FA buffer, overnight at 4°C. Following incubation, beads were washed twice with FA buffer, once with low salt wash buffer, once with high salt wash buffer, and once with TEL buffer before being eluted from beads using 100 ul of 1% SDS. Cross-linking was reversed by incubating samples at 65°C overnight in the presence of 20 mM NaCl, before protein and RNA were removed by RNAse A (30 min at 37°C) and Proteinase K (1 hour at 55°C) treatment. Samples were boiled at 95°C and DNA was purified using a Qiagen PCR purification kit, as per manufacturer's instructions.

Oxygen consumption assays

Oxygen consumption rate (OCR) was measured in worms using the Seahorse XF96 (Seahorse Bioscience) as previously described.[61] In brief, wildtype N2 worms were cultured on plates with control and *mtch-1*(RNAi) and grown till Day 1 and Day 3 of adulthood. On the day of analysis, Day 1 (YA) and Day 3 animals were transferred from respective NGM RNAi plates to plates without food to remove bacteria. Next, worms were transferred in 96-well Seahorse plates (approximately 10 worms per well and 10 such wells per condition tested) and OCR was measured 8 times. FCCP and Sodium Azide treatments were done at a final well concentration of 10 μM and 40 mM respectively. Mitochondrial (basal) and maximum OCR were measured for each condition. Data was normalised to worms per well.

Mitochondrial morphology assays

The mitochondria morphology in muscle of the *zcIs14[myo-3::GFP(mit)]* animals examined. 2% of molten agarose in water used to make glass slides. Animals were immobilized on agarose pads in 3 mM levamisole with a glass cover slip on the top. To acquire images, 63x/1.40 oil objective lens of the Zeiss Imager.Z2 microscope used. Images were processed using ImageJ. Qualitative analysis of the mitochondria morphology in each muscle section performed. The largest regions of clear body wall muscle were identified between the pharynx and the vulva or between the vulva and tail. No significant difference was observed between these two segments. Adjacent regions to the tail, pharynx and vulva were excluded due to the disrupted mitochondria morphology which naturally occurs there. Images scored as fused, tubular, intermediate and fragmented based on the mitochondria structure organization.

QUANTIFICATION AND STATISTICAL ANALYSIS

Sample number (n) corresponds to the number of biological replicates/trials or number of animals used, as stated in each figure legend. In all cases, Error bars correspond to SEM. All statistical tests (Mantel Cox Logrank, one-way ANOVA, two-way ANOVA and Student's t-test) were carried out as stated within each figure legend using GraphPad Prism 9. The statistical details of all experiments can be found within the accompanying figure legends and Table S1.